

Raman spectroscopy of self-catalyzed GaAs_{1-x}Sb_x nanowires grown on silicon

This content has been downloaded from IOPscience. Please scroll down to see the full text.

View [the table of contents for this issue](#), or go to the [journal homepage](#) for more

Download details:

IP Address: 128.178.106.14

This content was downloaded on 23/01/2014 at 04:21

Please note that [terms and conditions apply](#).

Raman spectroscopy of self-catalyzed GaAs_{1-x}Sb_x nanowires grown on silicon

Esther Alarcón-Lladó¹, Sònia Conesa-Boj¹, Xavier Wallart²,
Philippe Caroff^{2,3} and Anna Fontcuberta i Morral¹

¹ Laboratoire des Matériaux Semiconducteurs, École Polytechnique Fédérale de Lausanne, 1015 Lausanne, Switzerland

² Institut d'Électronique de Microélectronique et de Nanotechnologie, UMR CNRS 8520, Avenue Poincaré, BP 60069, F-59652 Villeneuve d'Ascq, France

³ Department of Electronic Materials Engineering, Australian National University, Canberra ACT 0200, Australia

E-mail: anna.fontcuberta-morral@epfl.ch and Philippe.caroff@anu.edu.au


Received 12 June 2013, in final form 31 July 2013

Published 12 September 2013

Online at stacks.iop.org/Nano/24/405707

Abstract

Thanks to their wide band structure tunability, GaAs_{1-x}Sb_x nanowires provide exciting perspectives in optoelectronic and energy harvesting applications. The control of composition and strain of these ternary alloys is crucial in the determination of their optical and electronic properties. Raman scattering provides information on the vibrational properties of materials, which can be related to the composition and strain. We present a systematic study of the vibrational properties of GaAs_{1-x}Sb_x nanowires for Sb contents from 0 to 44%, as determined by energy-dispersive x-ray analyses. We find that optical phonons red-shift with increasing Sb content. We explain the shift by alloying effects, including mass disorder, dielectric changes and ionic plasmon coupling. The influence of Sb on the surface optical modes is addressed. Finally, we compare the luminescence yield between GaAs and GaAs_{1-x}Sb_x, which can be related to a lower surface recombination rate. This work provides a reference for the study of ternary alloys in the form of nanowires, and demonstrates the tunability and high material quality of gold-free ternary antimonide nanowires directly grown on silicon.

 Online supplementary data available from stacks.iop.org/Nano/24/405707/mmedia

(Some figures may appear in colour only in the online journal)

1. Introduction

Antimonide-based III–V semiconductors are receiving much attention due to their promise for high-speed and low-power electronics, infrared optoelectronics, and thermophotovoltaic applications. Among many attractive properties, InAs_{1-x}Sb_x and GaAs_{1-x}Sb_x alloys present high electron and hole mobilities, bandgap tunability over a large range of the infrared spectrum, ranging from 1 to 12 μm , and original type I, II or III band alignments when grown as heterostructures with other III–V semiconductors [1–3].

On the other hand, the fabrication of antimonide-based nanowires is of great interest, not only for sub-wavelength phenomena, but also for the integration of mid-to-near IR optoelectronics with silicon technology. Additionally, the reduced dimensions provided by the nanoscale design enables

the combination of lattice-mismatched materials with minimal residual strain, thanks to an efficient elastic relaxation at the free borders and the interface. Unfortunately, the growth of GaAs_{1-x}Sb_x ternary alloy is challenging due to a large miscibility gap, $0.25 < x < 0.7$ [4]. It was found that either strain or non-equilibrium growth techniques, such as molecular beam epitaxy (MBE), can prevent phase segregation within this range [5, 6, 8]. There are only very few reports on GaAs_{1-x}Sb_x nanowires, all grown using the common gold-assisted growth mechanism [7]. Growth on silicon was achieved only as an axial segment inside a GaAs nanowire, but never reported as directly nucleated [9, 10]. To the best of our knowledge, no report on Raman spectroscopy of these ternary NWs has been published up to now.

Here we study ternary antimonide nanowires, which have been self-catalytically grown on a (111)-Si substrate

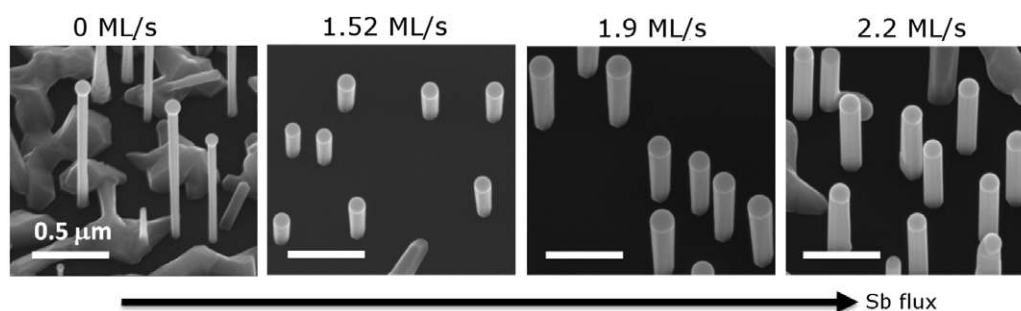


Figure 1. Representative scanning electron micrographs of four nanowire samples as-grown with different Sb fluxes. Scale bars are 500 nm.

by molecular beam epitaxy (MBE). Their optical properties have been investigated by using low-temperature micro-Raman and photoluminescence spectroscopy. We find that, as expected, an increase of Sb fraction x in an axial $\text{GaAs}_{1-x}\text{Sb}_x$ system yields a shift of the peak emission towards lower energy. The crystal structure and composition have been assessed by Raman spectroscopy. The results are compared to measurements realized with high-resolution transmission electron microscopy and energy-dispersive x-ray spectroscopy.

2. Experiment

All nanowires were grown on Si(111) substrates by solid source molecular beam epitaxy (MBE) at 630 °C. A silicon wafer piece was indium-stuck on an unpolished Si-substrate serving as a sample holder. A high-vacuum level was reached within less than 1 h after insertion and pumping down. The sample holder was degassed overnight at room temperature, mounted on a heater for further degassing at 250 °C for 2 h, then inserted into the reactor chamber. The nanowires were found to grow epitaxially, with a high vertical yield, on both the native-oxide-covered and oxide-free surfaces, as shown previously for GaAs nanowires [11]. Samples were not annealed at high temperature, but just brought to the growth temperature and stabilized for a few minutes prior to growth initiation. Growth was initiated immediately by simultaneously opening the gallium, arsenic and antimony shutters. Arsenic is in the form of an uncracked As_4 flux from a valved-cracker cell, a standard effusion cell is used for gallium and a valved-cracker cell is used for antimony, providing a Sb_2 molecular flux. Growth times were 30 min for all samples. The typical V/III ratio for pure GaAs nanowires was 1.9–2.2. The Ga flux was set to a 2D GaAs layer equivalent growth rate of 0.25 ML s^{-1} for all samples, while the As_4 and Sb_2 flux were varied to achieve composition tunability from 0% to 44% Sb. $\text{GaAs}_{1-x}\text{Sb}_x$ nanowires were grown by adding a nominal Sb_2 flux with 2D equivalent growth rates ranging from 0.20 to 2.17 ML s^{-1} (calibrated by induced RHEED oscillations during planar homoepitaxial GaSb layer growth). Growth was terminated by closing all shutters simultaneously and immediately switching off the power on the manipulator heater.

The morphology and dimensions of the nanowires were evaluated by scanning electron microscopy. The Sb atomic

content was obtained by energy-dispersive x-ray spectroscopy (EDX) using a FEI Tecnai OSIRIS microscope operated at 200 kV using a Super-X (0.9 rad collection angle) detector and Bruker Esprit software. Unpolarized micro-Raman scattering measurements were carried out at room temperature in the back-scattering configuration on single nanowires standing on the silicon substrate used for growth. The light beam was then parallel to the (111)B direction of the GaAsSb. One should note that, the nanowire density being relatively low, we expect light to interact with the entire nanowire axis [12]. The 520.8 nm line of an Ar–Kr⁺ laser was used as the excitation source. The incident and scattered light were focused through a 63× microscope objective ($\text{NA} = 0.75$). The scattered light was finally analyzed with a triple spectrometer equipped with a liquid nitrogen-cooled charge coupled device (CCD). The slit to the final stage was set to 50 μm , providing a spectral resolution down to 0.7 cm^{-1} . Photoluminescence measurements were performed with the same microscope setup by cooling the samples down to 7 K with a continuous flow helium cryostat and analyzing the emitted light by a single grating spectrometer and thermoelectrically cooled CCD. The PL spectra were corrected for the wavelength-dependent quantum efficiency of the CCD. The laser power used for optical experiments was around 25 kW cm^{-2} .

3. Results and discussion

3.1. Nanowire growth

We start by presenting the morphological evolution of the nanowires, starting with pure GaAs and while adding a flux of Sb_2 in the growth. Figure 1 shows representative scanning electron microscope images of four as-grown samples with Sb flux rates equivalent to growth rates of 0, 1.52, 1.9 and 2.2 ML s^{-1} . Starting with the pure GaAs case, nanowires exhibit a Ga droplet on the tip, responsible for the Ga-assisted VLS type of growth [11, 13]. Upon addition of a Sb_2 flux to the growth, the nanowire morphology is slightly affected in terms of length and diameter. We still observe a liquid droplet on the nanowire tip, however, a detailed analysis on the composition is out of the scope of this work and will be reported elsewhere. Interestingly, we see a reduction of the parasitic growth on the substrate and between the nanowires, which could be due to the surfactant effect of Sb and/or to a change in the effective V/III ratio [14].

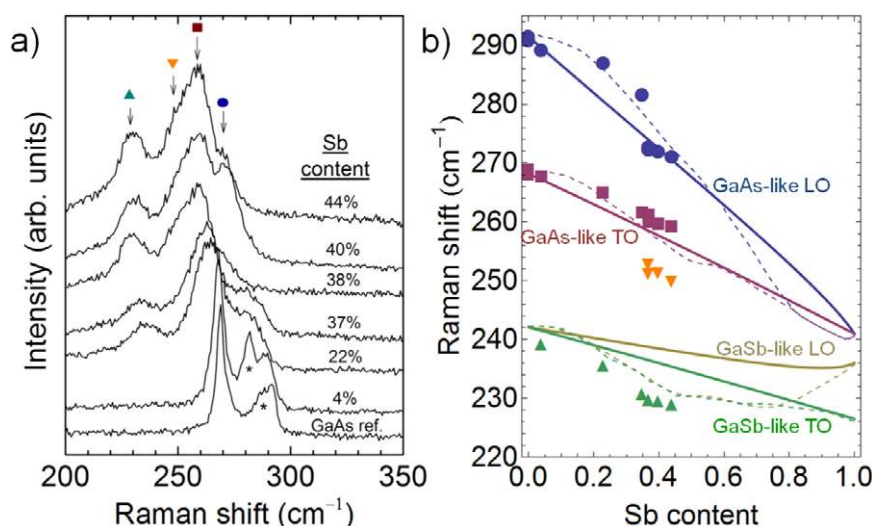


Figure 2. (a) Room-temperature Raman spectra of $\text{GaAs}_{1-x}\text{Sb}_x$ nanowires on a silicon substrate with increasing Sb content. The spectra are shifted for clarity. Alloy modes are marked by symbols and SO modes by an asterisk. (b) Alloy phonon mode frequencies as a function of Sb content. Experimental Raman frequencies are obtained from fitting the spectra to three (or four) Lorentzian functions. The Sb content is given from TEM-EDX. Solid lines correspond to the expected frequency calculated from the model described in the text. Dotted lines are data taken from thin films in [23].

3.2. Alloy phonon modes

We begin our analysis on the chemical composition of the $\text{GaAs}_{1-x}\text{Sb}_x$ nanowires by showing our Raman spectroscopy measurements on nanowires with different compositions, as measured by EDX. Figure 2(a) shows representative Raman spectra of the samples used in this work. In the back-scattering configuration from a (111) face of a zinc-blende crystal, both transverse and longitudinal optical modes (TO and LO, respectively) are allowed. Accordingly, the spectrum of the GaAs NWs reference sample is dominated by two peaks at around 268.8 and 291.5 cm^{-1} , which match the TO and LO modes of binary unstrained zinc-blende GaAs, respectively [15]. As predicted by out-of-resonance Raman selection rules, the TO intensity of the GaAs reference is around four times larger than that of the LO mode. Also, an intense shoulder at the low-frequency side of the LO peak marked with an asterisk in figure 2(a) is observed. As it will be discussed later on in further detail, we attribute this feature to a surface optical mode, which is widely observed in thin semiconductor nanowires such as the ones presented in this work [16, 17]. It is noteworthy that for all samples in this work, no signal of the wurtzite phase was detected, in contrast to what has been commonly found in long binary III–V nanowires such as GaAs, InAs and AlAs [18–23]. The Raman spectra of nanowires containing Sb are clearly different from that of bare GaAs NWs. First, both the GaAs TO and LO peaks shift to lower frequencies. This is the expected behavior in an alloy with an increasing concentration of a heavier atom in the lattice, as is the case for Sb with respect to As. Also, as the Sb content is increased, the two peaks significantly broaden, reflecting a higher degree of disorder. We also observe an additional peak around 230 cm^{-1} , which we attribute to the local vibration (LV) of GaSb in the GaAs lattice.

In order to analyze the Raman spectra in more detail, we have fitted them with Lorentzian lineshapes (see supplementary information available at stacks.iop.org/Nano/24/405707/mmedia). In figure 2(b), the peak frequencies obtained are depicted as a function of the Sb content, as obtained from the EDX measurements. One should note that the composition seems microscopically homogeneous along the nanowire axis (see further data later on this manuscript and in supplementary information available at stacks.iop.org/Nano/24/405707/mmedia). For comparison purposes, we have also plotted the alloy mode dependence found by McGlenn *et al* on $\text{GaAs}_{1-x}\text{Sb}_x$ thin films epitaxially grown on GaAs substrates [24]. In this work it was shown that the $\text{GaAs}_{1-x}\text{Sb}_x$ alloy system exhibits a two-mode behavior. From a vibrational point of view, any intermediate ternary alloy is constituted by two sets of phonon modes, each of them with frequencies close to one of the binaries, and their intensity scaling with the corresponding bond fraction. In the case of $\text{GaAs}_{1-x}\text{Sb}_x$, two sets of TO and LO phonons are observed. They are denominated GaAs-like and GaSb-like, with frequencies varying continuously from those for GaAs and GaSb respectively. At the end of the dependence and for very diluted alloys, the modes correspond to the local vibrational modes (LV) of the impurities (GaSb:As, GaAs:Sb, respectively). This two-mode and LV behavior has been observed for most of III–V alloys, such as AlGaAs, AlGaSb, GaAsP, InAlAs or InGaP [25, 26].

Our nanowires exhibit Sb compositions varying from 4% up to 44% according to EDX. As shown in figure 2(b), the positions of the GaAs-like TO and LO modes closely follow the trend measured in thin films. In the case of the GaSb-like mode, we were only able to detect the TO mode. This is expected, as stated earlier, since the intensity of the LO mode is much lower than that of the TO mode, the latter already being not very intense due to the relatively

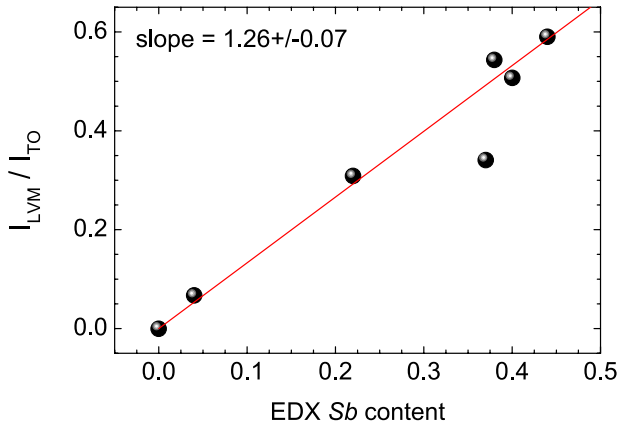


Figure 3. Normalized intensity of the GaSb-related mode as a function of Sb content. The red line is a linear fit to the represented data.

low concentration in Sb. The detailed understanding of the frequency shift of the TO and LO modes as a function of the Sb content requires one to look in more detail at the physics of phonons in ternary alloys, as described below. The position of both modes can be understood by following two different models, since they are mostly sensitive to different changes in the material (e.g. LO modes are generally more sensitive to electric fields). Under the virtual crystal approximation (VCA), an alloy such as $\text{GaAs}_{1-x}\text{Sb}_x$ can be treated like a continuum in the macroscopic scale whose physical properties linearly depend on the alloy composition, such as the lattice parameters and bond force constant (f) [24]. Thus, within the harmonic approximation, the square of the TO frequency will linearly shift from the frequency of the pure binary (i.e., GaAs) to the impurity mode of the oscillator surrounded by the other binaries (i.e., Ga–As in a GaSb matrix). The impurity mode (A in B) can be roughly estimated from $\omega_{A \text{ in B}}^{\text{TO}} = \omega_{\text{B}}^{\text{TO}} \sqrt{\mu_{\text{B}}/\mu_{\text{A}}}$, where μ_i and ω_i^{TO} are the reduced mass and TO frequency of the i th binary, respectively. This gives impurity mode frequencies of 251 cm^{-1} and 242 cm^{-1} for GaSb:As and GaAs:Sb, respectively, fitting relatively well to what has been measured. We have used this estimation for GaAs:Sb, while for GaSb:As we have adjusted it to the experimental value of $\sim 241 \text{ cm}^{-1}$ [8, 24]. On the other hand, following the theory of ionic plasmon coupling as described in [25], the dielectric function of an alloy is expressed as:

$$\varepsilon(\omega, x) = \varepsilon_{\infty}(x) + \sum_i \left(1 + \frac{\Omega_{\text{P},i}^2(x)}{\omega_{\text{TO},i}^2(x) - \omega^2} \right), \quad (1)$$

where $i = 1, 2$, $\varepsilon_{\infty}(x) = \varepsilon_{\infty,\text{A}}(1-x) + \varepsilon_{\infty,\text{B}}x$ is the dielectric constant of the mixed crystal and $\omega_{\text{TO},i}(x)$ and $\Omega_{\text{P},i}(x)$ are, respectively, the transverse optical frequency and the ionic plasma frequency of the i th sublattice in the alloy. The ionic plasma frequency of the sublattices takes into account the changes in the dielectric medium as well as transverse ionic charges of the oscillators. The LO mode frequencies of the alloy correspond to the zeros of the dielectric function. The solution to the above equation for the $\text{GaAs}_{1-x}\text{Sb}_x$ alloy is represented in figure 2(b) with solid lines. Our data

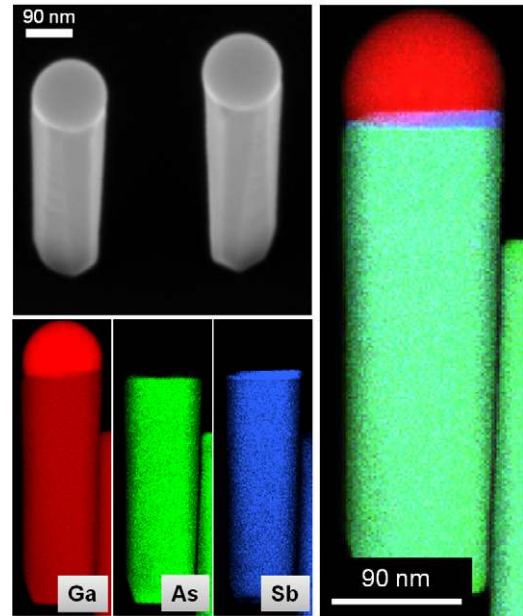


Figure 4. Scanning electron microscope image of $\text{GaAs}_{1-x}\text{Sb}_x$ NWs with $x \sim 40\%$ (top left). Energy-dispersive x-ray elemental image for a NW of the same sample (right picture), and its respective elemental maps for Ga, As and Sb (bottom left). A clear increased Sb content right below the droplet is observed.

follow quite well the frequency shift of the GaAs-like mode explained by mass disorder, a change in the dielectric medium and ionic plasma coupling associated with the alloying process. We find some small deviations in the dilute regime, which were also observed in previous works with thin films (dotted lines). Interestingly, the GaSb-like mode frequency differs from the theoretical dependence. We believe this might be due to a nonlinear evolution in the oscillator bond length.

We now would like to look in detail at the composition dependence of the GaSb-like or LV mode, as an alternative way of determining the Sb content. The relative intensity of the LV peak should scale linearly with the Sb atomic composition for As-rich $\text{GaAs}_{1-x}\text{Sb}_x$. In figure 3 we show the intensity of the LV mode relative to the GaAs-like TO as a function of the Sb content found from EDX measurements. From a linear fit, a correlation factor of 1.26 ± 0.07 was found. This relation results in an approximate quantification of the Sb content in $\text{GaAs}_{1-x}\text{Sb}_x$ material systems, for $x < 0.5$.

In the following, we discuss the additional features observed in the Raman spectra: alloy segregation for large Sb values detected by a shoulder in the GaAs-like TO mode towards lower frequencies and surface optical modes in the dilute regime.

3.3. Red-shifted TO GaAs-like peak in Sb-rich NWs

A broad shoulder to the low-frequency side of the GaAs-like TO peak is consistently observed for Sb contents above 37%. Asymmetrical LO modes were observed in previous works on $\text{GaAs}_{1-x}\text{Sb}_x$ thin films, and were attributed to phonon scattering with $q_{\text{ph}} \neq 0$ due to disorder. In our case, we believe this is not the source of the shoulder, even though

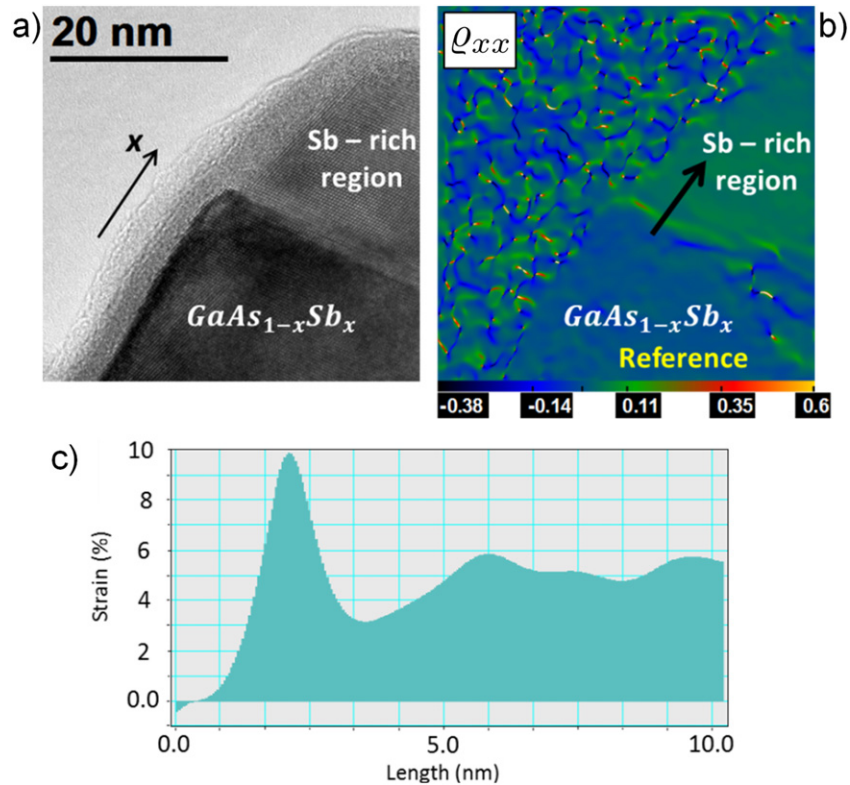


Figure 5. (a) Bright-field high-resolution TEM image of a $\text{GaAs}_{1-x}\text{Sb}_x$ ($x = 44\%$) nanowire exhibiting the Sb-rich region at the nanowire tip; (b) Q_{xx} relative strain map (or lattice mismatch) calculated with respect to the lower part region in the image, which corresponds to the NW body; (c) line profile performed in the Q_{xx} relative strain field map across the interface between $\text{GaAs}_{1-x}\text{Sb}_x$ and the Sb-rich region. The large mismatch between the NW body and the Sb-rich tip is rapidly relaxed after a few nanometers, leaving the rest of the Sb-rich region with an average relative mismatch of 5.8%.

disorder is obviously also present. In fact, out-of-zone center phonon scattering should be less relevant in the TO mode since its dispersion curve is flatter than that for the LO mode in GaAs [27]. On the other hand, regions with higher Sb content could give rise to a Raman peak at lower frequencies. In order to shed some light on this issue, high-resolution TEM-EDX maps of single NWs were performed. Figure 4 shows one of the maps on a sample with an Sb content of 40%. The elemental maps, as well as the combined one, clearly reveal an area right below the Ga droplet with a segment of Sb-rich $\text{GaAs}_{1-x}\text{Sb}_x$. The origin of this small segment has been confirmed to come from the post-growth precipitation of Sb and Ga from the droplet and will be investigated in more detail in a future publication. Even though the GaSb-rich region is small as compared to the rest of the NW, the actual cross-section is significant due to the tip position within the nanowire and the strong absorption of the $\text{GaAs}_{1-x}\text{Sb}_x$ NWs at the probing energy. The TEM-EDX data indicate that the alloy in this region exhibits an Sb content from 85–92%, for nanowires with respectively 35–44% of Sb in the core. Following the model described in section 3.2, the GaAs-like TO frequency for $\text{GaAs}_{1-x}\text{Sb}_x$ with $x = 85\text{--}92\%$ is expected around $245.2\text{--}243.2\text{ cm}^{-1}$, respectively—still lower than the experimental values. However, a high-resolution TEM analysis reveals that this region is, as one could expect, under strain. Figure 5 is an example of the strain analysis by HR-TEM for nanowires with the highest Sb content in

this work. From the high-resolution image of the nanowire tip (figure 5(a)), a map of the (111)-lattice parameter with respect to that of the nanowire body, or relative strain (Q_{xx}), can be obtained (figure 5(b)). It is clear from the relative strain map that the top region has a larger lattice parameter than that of the body, which contains less Sb. The lattice parameter of relaxed $\text{GaAs}_{0.08}\text{Sb}_{0.92}$ should be 3.7% larger than that of $\text{GaAs}_{0.56}\text{Sb}_{0.44}$. The TEM analysis gives an average relative difference of 5.8% along the (111) direction. The difference in lattice parameter between $\text{GaAs}_{0.08}\text{Sb}_{0.92}$ at the NW tip and the value for the relaxed material gives the absolute strain in the Sb-rich region. Thus, the absolute tensile strain, assuming Vegard's law for the $\text{GaAs}_{1-x}\text{Sb}_x$ alloy, is 1.93% along the growth direction (ϵ_{111}). Within the biaxial strain framework, the in-plane absolute strain ($\epsilon_{\text{in-plane}}$) is calculated and we obtain a value of -0.5% (see supplementary information for a detailed information on the strain calculations available at stacks.iop.org/Nano/24/405707/mmedia). These values are large enough to give rise to considerable shifts in the phonon frequencies. Assuming a linear change in the mechanical properties for $\text{GaAs}_{1-x}\text{Sb}_x$ [28], the strain-induced shift in the TO mode should be $\sim 3\text{ cm}^{-1}$ towards higher frequencies. This shift does not fully match the $\omega_{\text{TO}}^{\text{exp.}} - \omega_{\text{TO}}^{\text{model}} \sim 6\text{ cm}^{-1}$ from the Raman analysis, but is in good agreement within the average distance between model and experimental TO frequencies from the NW bodies.

Table 1. Summary of the surface optical mode frequencies observed for GaAs_{1-x}Sb_x NWs with $x = 0$ and 4%, calculated as described in the text. The frequency in parenthesis refers to that obtained after continuous laser exposure. All frequencies are given in cm⁻¹. The diameter of measured NWs is from 40 to 60 nm. The theoretical values are obtained for cylindrical NWs with $r = 25$ nm.

	$\omega_{\text{SO}}^{\text{exp.}}$	$\omega_{\text{SO}}^{\text{calc.}}$	
		In air	In Ga ₂ O ₃
GaAs NWs	286.5 (280.4)	288.9	278.1
GaAs _{0.96} Sb _{0.04} NWs	281.6	287.4	276.9

3.4. Surface optical modes and photoluminescence in As-rich NWs

Finally, we want to address the Raman features marked with an asterisk in figure 2(a) in the spectra of pure GaAs and GaAs_{0.96}Sb_{0.04} NWs. Additional peaks in the first-order Raman spectrum with frequencies between the TO and LO modes have been previously observed in several III–V nanowires and identified as surface optical (SO) modes [17, 29–31]. Surface modes are determined by the dielectric properties of the materials on both sides of the surface as well as by the surface geometry itself [32]. A simple expression is given for finding the SO frequency in a material of cylindrical shape with radius r embedded in a dielectric medium (ϵ_m) [30]:

$$\varepsilon(\omega) + \varepsilon_m \frac{I_0(qr)K_1(qr)}{I_1(qr)K_0(qr)} = 0, \quad (2)$$

where $\varepsilon(\omega)$ is the dielectric function of GaAs, I_i and K_i are the modified Bessel functions and q is the phonon wavevector. From this equation, we find an SO mode frequency of 288.9 cm⁻¹ for GaAs NWs of 50 nm in diameter embedded in air, by using $4\pi n\lambda = 10^6$ cm⁻¹ ($\lambda = 520.8$ nm and the refractive index was taken from [33]). This is slightly larger than the experimental value of 286.5 cm⁻¹ and might arise from a hexagonal NW cross-section instead of a cylindrical one. Interestingly, the Raman spectrum of GaAs_{0.96}Sb_{0.04} nanowires also seems to reveal an SO mode. For larger Sb contents, the alloy modes are too broad to enable the clear observation of such features. The SO mode is now red-shifted from that of the pure GaAs, like the rest of the alloy modes. From the equation above, using now the effective dielectric constant and the TO frequency of the alloy as described in section 3.3, a frequency of 287.4 cm⁻¹ is obtained for NWs of 50 nm in diameter and 4% of Sb. Again, the calculated frequency is higher than the experimental value. The experimental and calculated frequencies are summarized in table 1.

On the other hand, it is well known that the GaAs surface is not stable and an oxide layer may form. Because SO modes are confined at the surface, their frequency is very sensitive to surface changes. A layer of gallium oxide surrounding the nanowire will definitely change the vibration of the surface mode. Laser induced changes have been observed in GaAs nanowires in previous works [34]. In this work, however, we are not forming crystalline arsenic, but the oxidation of Ga is anticipated at the NW surface, which might be

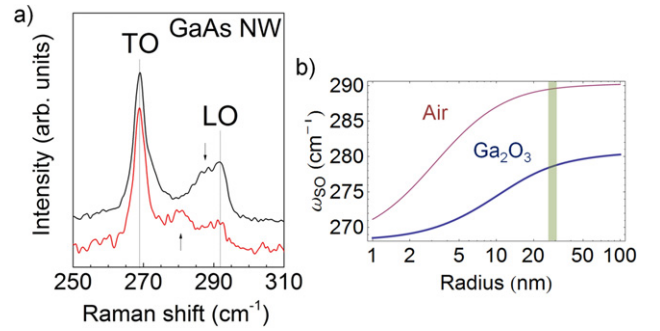


Figure 6. (a) Raman spectra of a GaAs NW (black curve) showing the SO mode at 287.6 cm⁻¹. The red curve is the spectrum of the same wire after persistent light exposure, revealing a red-shift in the SO peak. (b) SO frequency as a function of NW radius calculated from the expression and parameters in the text. The upper curve has been obtained for NWs surrounded by air while the dielectric constant of Ga₂O₃ has been used for the lower curve. The shaded area represents the range of NW diameters dealt with in this work.

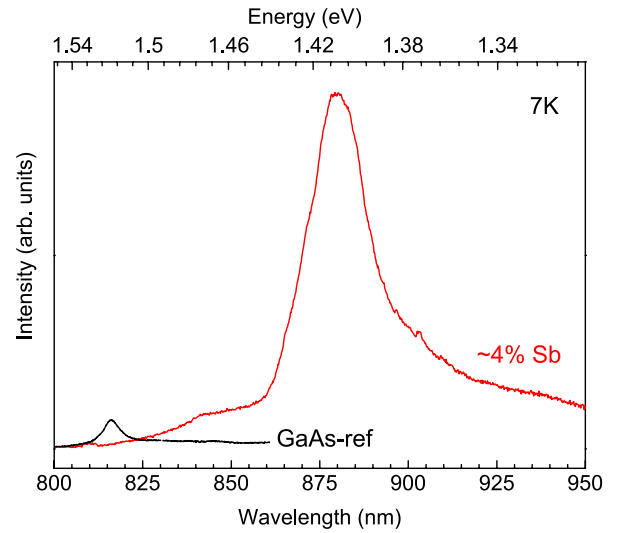


Figure 7. Photoluminescence (PL) spectrum of the GaAs_{1-x}Sb_x NWs with the lowest Sb content in this work. The PL of GaAs reference NWs grown with the same system is also shown.

triggered by laser radiation. Indeed, we observed changes in the SO signal after persistent laser exposure of GaAs NWs. In figure 6(a) we have plot two Raman spectra of the same GaAs nanowire, before and after laser exposure. While no apparent changes happen for the TO and LO peaks, the SO mode has significantly red-shifted. We believe that the red-shift might arise from changes in the surrounding dielectric constant due to surface oxidation. To illustrate the effect of oxide formation on the SO mode, we have plotted in figure 6(b) the surface mode frequency as a function of radius for two different surrounding media, air ($\epsilon_m = 1$) and Ga₂O₃ ($\epsilon_m = 10.2$) [35]. Due to the much larger permittivity of gallium oxide, the frequency of the surface optical mode is strongly reduced.

Lastly, we show the low-temperature photoluminescence (PL) spectra of a GaAs reference NW along with that of a GaAs_{0.96}Sb_{0.04} NW taken at the same power excitation (figure 7). The measurements were realized in the same

configuration as in Raman measurements, and both kinds of nanowires exhibited comparable dimensions. The PL spectrum of the reference sample is dominated by the free exciton at 1.52 eV and defect-mediated exciton recombination at lower energies (around 1.5 eV) [36]. As expected, the emission of the GaAs_{0.96}Sb_{0.04} NW is at a lower energy and surprisingly more than ten times stronger than that of the reference GaAs NW. The main PL peak is centered at 1.4 eV, and weaker emissions at both higher and lower energies are detected. Photoluminescence in thin GaAs nanowires is known to be strongly quenched by surface-related defects [37, 38], and has been proved to improve when passivated with semiconducting polymers [39]. Thus, we believe that the increase in PL intensity of more than one order of magnitude in low-doped GaAs NWs is due, at least in part, to the passivation properties of antimonides. Cross-section EDX investigations (not shown) did not reveal any detectable gradient of Sb towards the surface. This effect should be investigated in more detail in the future.

4. Conclusion

In conclusion, we have investigated by Raman spectroscopy GaAs_{1-x}Sb_x nanowires with an antimony content between 4 and 44%. We observe the shift on the optical phonons due to alloying effects, including mass disorder, dielectric changes and ionic plasmon coupling. Surface modes are also detected. For samples with 4% Sb content, we observe more than one order of magnitude increase in the intensity of luminescence, which we attribute to a reduction of the surface recombination rate with the slight presence of Sb during growth. This study represents a base for future structural studies on ternary nanowire-based alloys.

Acknowledgments

EAL acknowledges funding from the Marie Curie Actions Program. SCB acknowledges funding from the Marie Heim-Vögtlin program project PMPDP2-139702. AFM is grateful for funding through the ERC Starting Grant UpCon and NCCR-QSIT. PC is the recipient of an Australian Research Council Future Fellowship (project number FT120100498).

References

- [1] Liu C, Li Y and Zeng Y 2010 *Engineering* **2** 617
- [2] Fras L M, Avery J E, Sundaram V S, Dinh V T, Davenport T M, Yerkes J W, Gee J M and Emery K A 1990 *Proc. 21st IEEE PV Specialist Conf.* p 190
- [3] Aardvark A, Mason N J and Walker P J 1997 *Prog. Cryst. Growth Charact.* **35** 207
- [4] Stringfellow G B 1982 *J. Electron. Mater.* **11** 903
- [5] Cherng M J, Stringfellow G B and Cohen R M 1984 *Appl. Phys. Lett.* **44** 677
- [6] Chang C-A, Ludeke R, Chang L L and Esaki L 1977 *Appl. Phys. Lett.* **31** 759
- [7] Dheeraj D L, Patriarche G, Largeau L, Zhou H L, van Helvoort A T J, Glas F, Harmand J C, Fimland B O and Weman H 2008 *Nanotechnology* **19** 275605
- [8] Toda T, Nishino F, Kato A, Kambayashi T, Jinbo Y and Uchitomi N 2006 *Phys. B* **376** 602
- [9] Plissard S, Dick K A and Caroff P 2010 *Appl. Phys. Lett.* **96** 121901
- [10] Munshi A M, Dheeraj D L, Todorovic J, van Helvoort A T J, Weman H and Fimland B-O 2013 *J. Cryst. Growth* **372** 163
- [11] Plissard S, Dick K A, Larrieu G, Godey S, Addad A, Wallart X and Caroff P 2010 *Nanotechnology* **21** 385601
- [12] Krogstrup P, Jorgensen H I, Heiss M, Demichel O, Holm J V, Aagesen M, Nygard J and Morral A F I 2013 *Nature Photon.* **7** 306
- [13] Colombo C, Spirkoska D, Frimmer M, Abstreiter G and Morral A F I 2008 *Phys. Rev. B* **77** 155326
- [14] Horn-vonHoegen M, LeGoues F K, Copel M, Reuter M C and Tromp R M 1991 *Phys. Rev. Lett.* **67** 1130
- [15] Yu P Y and Cardona M 1996 *Fundamentals of Semiconductors* (Berlin: Springer)
- [16] Bohren C F and Huffman D R 2004 *Absorption and Scattering of Light by Small Particles* (New York: Wiley)
- [17] Spirkoska D, Abstreiter G and Morral A F I 2008 *Nanotechnology* **19** 435704
- [18] Glas F, Harmand J-C and Patriarche G 2007 *Phys. Rev. Lett.* **99** 146101
- [19] Spirkoska D *et al* 2009 *Phys. Rev. B* **80** 245325
- [20] Funk S, Li A, Ercolani D, gemmi M, Sorba L and Zardo I 2013 *ACS Nano* **7** 1400
- [21] Hormann N G, Zardo I, Hertenberger S, Funk S, Bolte S, Doblinger M, Koblmueller G and Abstreiter G 2011 *Phys. Rev. B* **84** 155301
- [22] Ketterer B, Uccelli E and Morral A F I 2012 *Nanoscale* **4** 1789
- [23] Caroff P, Dick K A, Johansson J, Messing M E, Deppert K and Samuelson L 2009 *Nature Nanotechnol.* **4** 50
- [24] McGlenn T C, Krabach T N, Klein M V, Bajor G, Greene J E, Kramer B, Barnett S A, Lastras A and Gorbatkin S 1986 *Phys. Rev. B* **33** 8396
- [25] Groenen J, Carles R, Landa G, Guerret-Piecourt C, Fontaine C and Gendry M 1998 *Phys. Rev. B* **58** 10452
- [26] Pages O, Souhabi J, Postnikov A V and Chafi A 2009 *Phys. Rev. B* **80** 035204
- [27] Strauch D and Dorner B 1990 *J. Phys.: Condens. Matter* **2** 1457
- [28] Vurgaftman I, Meyer J R and Ram-Mohan L R 2001 *J. Appl. Phys.* **89** 5815
- [29] Lin H-M, Chen Y-L, Yang J, Liu Y-C, Yin K-M, Kai J-J, Chen F-R, Chen L-C and Chen C-C 2003 *Nano Lett.* **3** 537
- [30] Gupta R, Xiong Q, Mahan G D and Eklund P C 2003 *Nano Lett.* **3** 1745
- [31] Mata R, Cros A, Hestroffer K and Daudin B 2012 *Phys. Rev. B* **85** 035322
- [32] Adu K W, Xiong Q, Gutierrez H R, Chen G and Eklund P C 2006 *Appl. Phys. A* **85** 287
- [33] Aspnes D E and Studna A A 1983 *Phys. Rev. B* **27** 985
- [34] Yazji S, Zardo I, Soini M, Postorino P, Morral A F I and Abstreiter G 2011 *Nanotechnology* **22** 325701
- [35] Passlack M, Schubert E F, Hobson W S, Hong M, Moriya N, Chu S N G, Konstadinidis K, Mannaerts J P, Schnoes M L and Zydzik G J 1995 *J. Appl. Phys.* **77** 686
- [36] Parkinson P, Lloyd-Hughes J, Gao Q, Tan H H, Jagadish C, Johnston M B and Herz L M 2007 *Nano Lett.* **7** 2162
- [37] Demichel O, Heiss M, Bleuse J, Mariette J and Morral A F I 2010 *Appl. Phys. Lett.* **97** 201907
- [38] Joyce H, Docherty C J, Gao Q, Tan H H, Jagadish C, Lloyd-Hughes J, Herz L M and Johnston M B 2013 *Nanotechnology* **24** 214006
- [39] Yong C K, Noori K, Gao Q, Joyce H J, Tan H H, Jagadish C, Giustino F, Johnston M and Herz L M 2012 *Nano Lett.* **12** 6293